AGU PUBLICATIONS

Global Biogeochemical Cycles

RESEARCH ARTICLE
10.1002/2014GB005017

Key Points:
- Global dissolved iron flux from margin sediments of 109 ± 55 Gmol yr^{-1}
- Benthic dissolved iron flux has been underestimated in the marine iron cycle
- Iron scavenging rates in water column probably higher than currently presumed

Supporting Information:
- Text S1, Figure S1, and Tables S1–S5

Correspondence to:
A. W. Dale,
adale@geomar.de

Citation:
Dale, A. W., L. Nickelsen, F. Scholz, C. Hensen, A. Oschlies, and K. Wallmann (2015), A revised global estimate of dissolved iron fluxes from marine sediments, *Global Biogeochem. Cycles*, *29*, 691–707, doi:10.1002/2014GB005017.

Received 15 OCT 2014
Accepted 2 APR 2015
Accepted article online 7 APR 2015
Published online 28 MAY 2015

A revised global estimate of dissolved iron fluxes from marine sediments

A. W. Dale[1], L. Nickelsen[1], F. Scholz[1], C. Hensen[1], A. Oschlies[1], and K. Wallmann[1]

[1]GEOMAR Helmholtz Centre for Ocean Research Kiel, Kiel, Germany

Abstract Literature data on benthic dissolved iron (DFe) fluxes (μmol m^{-2} d^{-1}), bottom water oxygen concentrations (O_{2BW}, μM), and sedimentary carbon oxidation rates (C_{OX}, mmol m^{-2} d^{-1}) from water depths ranging from 80 to 3700 m were assembled. The data were analyzed with a diagenetic iron model to derive an empirical function for predicting benthic DFe fluxes: DFe flux $= \gamma \cdot \tanh\left(\frac{C_{OX}}{O_{2BW}}\right)$ where γ (= 170 μmol m^{-2} d^{-1}) is the maximum flux for sediments at steady state located away from river mouths. This simple function unifies previous observations that C_{OX} and O_{2BW} are important controls on DFe fluxes. Upscaling predicts a global DFe flux from continental margin sediments of 109 ± 55 Gmol yr^{-1}, of which 72 Gmol yr^{-1} is contributed by the shelf (<200 m) and 37 Gmol yr^{-1} by slope sediments (200–2000 m). The predicted deep-sea flux (>2000 m) of 41 ± 21 Gmol yr^{-1} is unsupported by empirical data. Previous estimates of benthic DFe fluxes derived using global iron models are far lower (approximately 10–30 Gmol yr^{-1}). This can be attributed to (i) inadequate treatment of the role of oxygen on benthic DFe fluxes and (ii) improper consideration of continental shelf processes due to coarse spatial resolution. Globally averaged DFe concentrations in surface waters simulated with the intermediate-complexity University of Victoria Earth System Climate Model were a factor of 2 higher with the new function. We conclude that (i) the DFe flux from marginal sediments has been underestimated in the marine iron cycle and (ii) iron scavenging in the water column is more intense than currently presumed.

1. Introduction

Iron (Fe) is a regulating micronutrient for phytoplankton productivity and the efficiency of the biological pump over large areas of the ocean [*Martin and Fitzwater*, 1988; *Martin*, 1990; *Moore and Doney*, 2007; *Boyd and Ellwood*, 2010]. Natural iron fertilization by enhanced dust inputs is believed to have contributed to lower CO_2 levels during the Last Glacial Maximum [*Martin*, 1990; *Sigman and Boyle*, 2000]. Understandably, therefore, global circulation models with a focus on Fe have often considered dissolution from dust to be the major external source of dissolved iron to the surface ocean [*Archer and Johnson*, 2000; *Aumont et al.*, 2003; *Parekh et al.*, 2004]. The atmospheric, dissolvable iron input is around 10 Gmol yr^{-1} or less, yet is highly uncertain due to the poorly constrained solubility of particulate iron [*Jickells et al.*, 2005; *Luo et al.*, 2008; *Mahowald et al.*, 2005; *Galbraith et al.*, 2010; *Misumi et al.*, 2014; *Nickelsen et al.*, 2015].

More recently, continental margin sediments have been shown to be important sources of dissolved iron (DFe) to the coastal ocean and beyond [*Elrod et al.*, 2004; *Lohan and Bruland*, 2008; *Cullen et al.*, 2009; *Severmann et al.*, 2010; *Jeandel et al.*, 2011; *John et al.*, 2012; *Conway and John*, 2014]. Most global iron models now include an explicit sediment source of DFe, albeit with very different parameterizations. For instance, benthic DFe fluxes have been described using a fixed or maximum flux at the seafloor [*Moore et al.*, 2004; *Aumont and Bopp*, 2006; *Misumi et al.*, 2014]. Others used the empirical relationship between DFe flux and benthic carbon oxidation rates (C_{OX}) proposed by *Elrod et al.* [2004] [*Moore and Braucher*, 2008; *Palastanga et al.*, 2013]. In recognition that DFe fluxes from marine sediments are enhanced under oxygen-deficient bottom waters [*McManus et al.*, 1997; *Lohan and Bruland*, 2008; *Severmann et al.*, 2010], some workers opted for an oxygen "switch" [*Galbraith et al.*, 2010; *Nickelsen et al.*, 2015]. Here, all particulate iron that falls to the seafloor is returned to the water column as DFe if bottom water oxygen concentration (O_{2BW}) falls below a predefined threshold. Given the lack of consensus of how benthic iron should be described in models, the magnitude of this source is only vaguely constrained at 8–32 Gmol yr^{-1} [*Jickells et al.*, 2005; *Galbraith et al.*, 2010; *Misumi et al.*, 2014; *Nickelsen et al.*, 2015; *Tagliabue et al.*, 2014]. This uncertainty is very likely propagated to the parameterization of the DFe source/sink terms in the water column, which themselves are very poorly understood [*Nickelsen et al.*, 2015]. Thus, there is a real need to better constrain DFe sources and sinks in the ocean.

Table 1. Literature Data on Benthic DFe Fluxes

Region	Water Depth[a] (m)	O_2 (μM)	C_{OX} (mmol m^{-2} d^{-1})	DFe Flux (μmol m^{-2} d^{-1})	Remarks
Californian margin and Borderland Basins[b]	100–3700	8–138	0.3–7.3	0.02–48	Highest fluxes with shallow oxygen penetration depths
Monterey Bay (California)[c]	100	101–185	6.9–14.7	1.3–10.8	Interannual and intraannual variability at a single station
Oregon-California shelf and Californian Borderland Basins[d]	90–900	3–153	2–23	12–568	High fluxes for Eel River mouth and San Pedro and Santa Monica Basins, temporal variability
Peruvian margin[e]	95–400	< d.l	2.4–7.7	11–888	Highest flux measured for an open margin setting

[a]Depth range where the data were collected.
[b]*McManus et al.* [1997]: Total dissolved iron determined by chemiluminescence. Positive fluxes only (= out of sediment). Negative fluxes are <0.5 μmol m^{-2} d^{-1} and ignored in this study. C_{OX} was determined from ΣCO_2 fluxes corrected for carbonate dissolution.
[c]*Berelson et al.* [2003]: Total dissolved iron determined by flow injection analysis with chemiluminescence detection. C_{OX} was determined from ΣCO_2 fluxes corrected for carbonate dissolution.
[d]*Severmann et al.* [2010]: Total dissolved iron determined by inductively coupled plasma mass spectrometry. DFe fluxes of 421 to 568 μmol m^{-2} d^{-1} were reported for the San Pedro and Santa Monica Basins compared to only 13–18 μmol m^{-2} d^{-1} measured previously at the same sites (reported by *Elrod et al.* [2004]). C_{OX} was determined from ΣCO_2 fluxes without correction for carbonate dissolution.
[e]*Noffke et al.* [2012]: Total dissolved iron determined by inductively coupled plasma mass spectrometry. C_{OX} was determined as the HCO_3^- flux from pore water total alkalinity gradients and showed very good agreement with numerical modeling results [*Bohlen et al.*, 2011].

While there is little disagreement that both O_{2BW} and C_{OX} are important factors for predicting DFe fluxes, a unifying paradigm has so far not been proposed in a quantitative and empirical fashion. The oxygen threshold used by *Galbraith et al.* [2010] and *Nickelsen et al.* [2015] is an advance in the right direction, but the threshold concentration is somewhat arbitrary and not well justified empirically. In this study, we reanalyze the available literature data at sites where benthic DFe fluxes, O_{2BW}, and C_{OX} have been reported. Our prime objective is to derive a simple algorithm to predict DFe fluxes from marine sediments at the global scale based on O_{2BW} and C_{OX} as the two key controlling variables. We then analyze the impact of this source on DFe distributions in ocean surface waters by coupling the algorithm to the intermediate-complexity University of Victoria Earth System Climate Model (UVic ESCM). We find that the sedimentary DFe source may be several times higher than current estimates suggest, implying that scavenging in the water column is currently too weak in global iron models and that the residence time of iron in the ocean is shorter than assumed previously.

2. Data Acquisition and Evaluation

Benthic iron fluxes were compiled from the literature along with reported O_{2BW} and C_{OX} (Table 1). In these studies, the water samples for iron analysis were filtered (0.45 μm), acidified, and analyzed for the total dissolved fraction using various analytical methodologies (see Table 1). Only fluxes measured using non-invasive benthic chambers were considered. DFe fluxes derived from pore water gradients often do not correlate with in situ fluxes due to processes at the sediment-water interface operating over spatial scales smaller than the typical centimeter-scale sampling resolution [e.g., *Homoky et al.*, 2012]. Furthermore, enhanced DFe flux to the bottom water by flushing of animal burrows (bioirrigation) is also not captured by pore water gradients. We note, however, that benthic DFe fluxes determined using chambers may also suffer from artifacts due to oxidative losses and scavenging onto particles [e.g., *Severmann et al.*, 2010]. In this study, we make no attempt to reevaluate the published data with regards to these aspects and the reported benthic DFe fluxes are used.

Almost all data where DFe fluxes, O_{2BW}, and C_{OX} have been measured simultaneously originate from the Californian shelf and slope [*McManus et al.*, 1997; *Berelson et al.*, 2003; *Severmann et al.*, 2010]. These data cover a wide range of C_{OX} and O_{2BW} from severely hypoxic (~3 μM) to normal oxic (>63 μM) conditions. DFe fluxes range from <0.1 μmol m^{-2} d^{-1} on the slope to 568 μmol m^{-2} d^{-1} in the San Pedro Basin. High fluxes of 332 μmol m^{-2} d^{-1} were also measured on the Oregon margin close to river mouths [*Severmann et al.*, 2010]. Absent from the Californian data are DFe fluxes under anoxic conditions. In situ fluxes are available for anoxic areas of the Baltic and Black Seas [*Friedrich et al.*, 2002; *Pakhomova et al.*, 2007]. Yet these are not included in our database because supporting C_{OX} data are unfortunately lacking. We therefore supplemented the database with fluxes from the Peruvian oxygen minimum zone where bottom waters on the shelf and upper slope are predominantly anoxic [*Noffke et al.*, 2012]. The highest DFe flux in

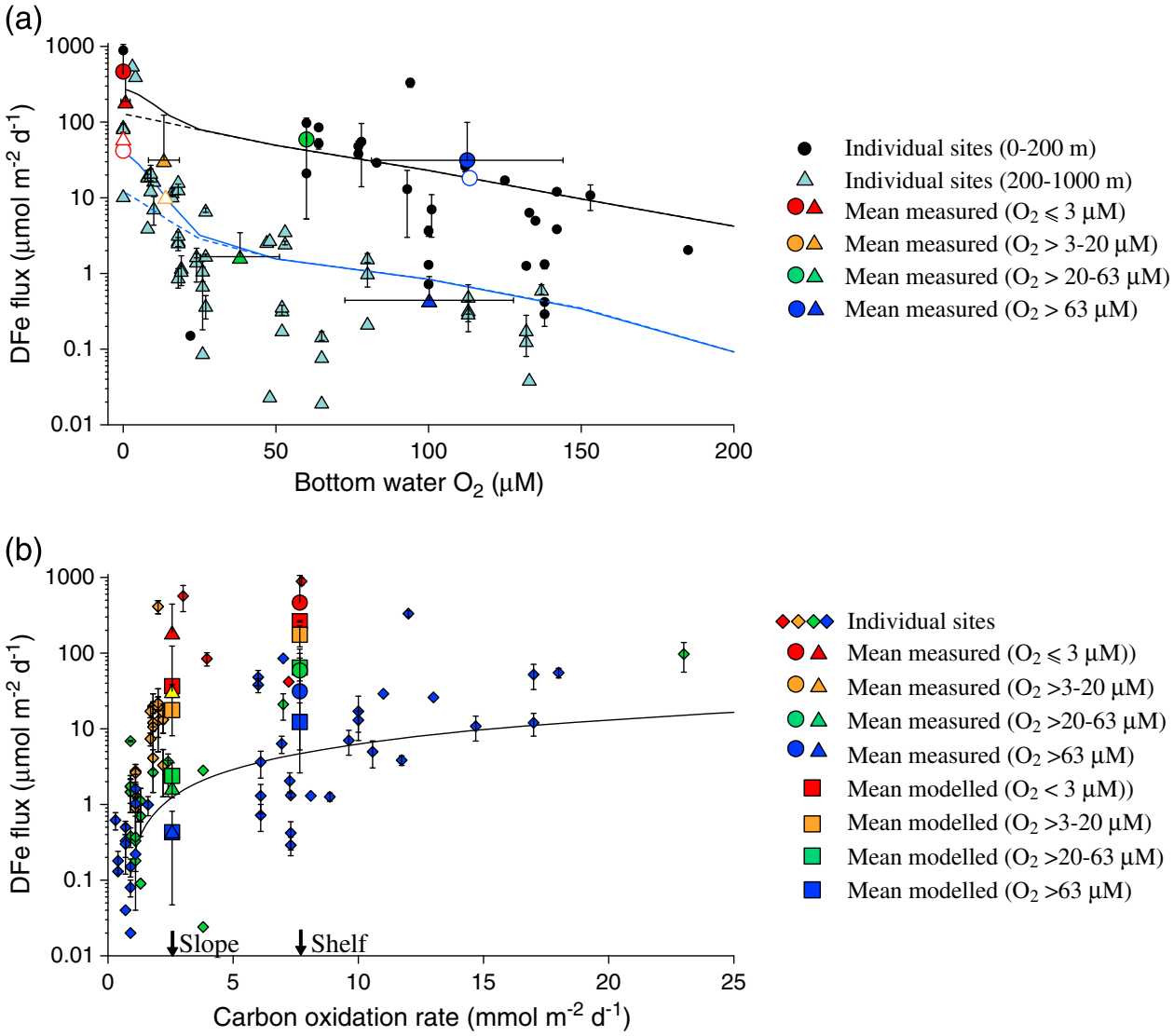

Figure 1. (a) Measured DFe fluxes versus bottom water O_2. Black circles and light blue triangles correspond to individual sites with $C_{OX} > 4$ (≈ shelf) and <4 mmol m^{-2} d^{-1} (≈ slope), respectively. The larger colored symbols are the mean DFe fluxes and O_2 concentrations within each binned range of O_2 (error bars are standard deviations), where circles and triangles denote shelf and slope, respectively. The large white symbols with colored outlines show the binned data without the four fluxes >300 µmol m^{-2} d^{-1} (San Pedro Basin, Santa Monica Basin, Eel River shelf, and Peruvian shelf). The black and blue curves are modeled fluxes for the shelf and slope, respectively; solid curves = standard model and dashed lines = standard model with no decrease in faunal activity at low O_{2BW}. (b) Measured DFe fluxes versus C_{OX} color coded according to O_{2BW} (diamonds). The large circles (shelf) and triangles (slope) are the measured binned data from Figure 1a plotted for the shelf and slope values of C_{OX} (indicated on the *x* axis). The mean modeled fluxes for each O_{2BW} interval are the corresponding colored squares. The curve is the regression of *Elrod et al.* [2004]: $DFe = 0.68 \times C_{OX} - 0.5$, based on data published by *McManus et al.* [1997] and *Berelson et al.* [2003]. Error bars for the individual sites in Figures 1a and 1b are taken from the literature where reported (Table 1). Error bars on C_{OX} are not shown for clarity.

our database was measured here (888 µmol m^{-2} d^{-1}). In this study, we define anoxia as O_2 concentrations below the detection limit of the Winkler titration, approximately 3 µM.

The final database includes 81 data points where DFe flux, O_{2BW}, and C_{OX} data have been reported for the same site. DFe fluxes and C_{OX} were taken as the reported mean values plus error (where given) determined from multiple chambers during the same deployment. Hence, the actual number of individual DFe fluxes is much greater than 81. In total, 25 fluxes are from shelf settings (≤200 m), 40 are from the slope (>200–2000 m), and 16 are from deeper waters down to 3700 m. The deep sea is thus underrepresented in the database compared to the continental margin.

At first glance, defining any relationship between DFe flux, O_{2BW}, and C_{OX} seems like an impossible task (Figure 1). DFe fluxes scatter over many orders of magnitude for any given O_{2BW} or C_{OX}. The apparent dependence of DFe flux on O_{2BW}, as observed in the data set of *Severmann et al.* [2010], is much more tenuous when data from all studies are considered collectively. The linear relationship between DFe flux (in $\mu mol\,m^{-2}\,d^{-1}$) and C_{OX} (in $mmol\,m^{-2}\,d^{-1}$) proposed by *Elrod et al.* [2004] does seem to broadly apply ($DFe = 0.68 \times C_{OX} - 0.5$), although DFe fluxes $>10\,\mu mol\,m^{-2}\,d^{-1}$ for low C_{OX} are not well represented by that model (Figure 1b).

In order to understand the scatter in these plots, we first organized the individual fluxes into two groups depending on whether the C_{OX} was above or below $4\,mmol\,C\,m^{-2}\,d^{-1}$. This definition is not arbitrary; it represents the C_{OX} at the shelf break (approximately 200 m) where a sharp gradient change in total benthic O_2 uptake occurs [*Andersson et al.*, 2004]. Above this depth (i.e., on the shelf), C_{OX} increases to $>20\,mmol\,m^{-2}\,d^{-1}$, whereas on the slope it declines much more gradually to approximately $1\,mmol\,m^{-2}\,d^{-1}$ or less at 3000 m [*Burdige*, 2007]. Although we recognize that C_{OX} does not strictly correlate with water depth, the overall relationship is clear enough [see *Burdige*, 2007] that we can collectively term the sites above and below the C_{OX} threshold as shelf and slope, respectively.

In a second step, the DFe fluxes were binned into discrete O_{2BW} intervals: anoxic ($O_{2BW} \leq 3\,\mu M$), severely hypoxic ($>3\,\mu M < O_{2BW} \leq 20\,\mu M$), weakly hypoxic ($>20\,\mu M < O_{2BW} \leq 63\,\mu M$), and normal oxic ($O_{2BW} > 63\,\mu M$). Two of these boundaries were chosen based on strict (i.e., anoxia, that is, below detection limit) or more consensual definitions (i.e., hypoxia = $O_2 < \sim 63\,\mu M$). The $20\,\mu M$ boundary is somewhat subjective. We chose this value because *Elrod et al.* [2004] noted that their DFe-C_{OX} correlation did not capture iron fluxes at sites with O_{2BW} concentrations below this value. It may well be that this concentration represents a tipping point beyond which large changes in DFe flux occur due to alterations in respiration pathways and/or faunal regime shifts [*Levin and Gage*, 1998]. We will revisit this idea later.

Following these criteria, the data broadly show that DFe flux correlates inversely with increasing O_{2BW} and decreasing C_{OX}. High DFe fluxes on the shelf (circles in Figure 1a) are clearly distinguishable from the much lower fluxes on the slope (triangles). For the slope setting, low DFe fluxes of 1.3 and $0.4\,\mu mol\,m^{-2}\,d^{-1}$ are found for the weakly hypoxic and oxic intervals, respectively, whereas a pronounced increase to 36 and $188\,\mu mol\,m^{-2}\,d^{-1}$ is associated with the severely hypoxic and anoxic intervals (respectively). A very similar trend emerges for the shelf with a high-end flux of $465\,\mu mol\,m^{-2}\,d^{-1}$ in anoxic shelf settings. However, there is a large uncertainty associated with these numbers due to (i) few data available for anoxic and hypoxic sites on the shelf and (ii) bias toward the high fluxes measured in the San Pedro and Santa Monica Basins and on the Peru and Eel River shelves. Excluding these four points with DFe fluxes $>300\,\mu mol\,m^{-2}\,d^{-1}$ considerably reduces the binned values for anoxic and severely hypoxic waters (open symbols in Figure 1a). Furthermore, it is also not clear if the high fluxes on the shelf truly reflect higher C_{OX} or whether this simply reflects the fact that most organic matter is deposited on the shelf along with iron-rich terrestrial material. Consequently, in the following section we use a diagenetic model to identify the factors regulating benthic iron fluxes and provide a mechanistic understanding of the emerging trends in Figure 1.

3. Benthic Iron Model

A vertically resolved 1-D reaction-transport model was used to simulate the coupled C, N, Fe, Mn, and S cycles in the upper 30 cm of sediments. Our aim is to calculate benthic DFe fluxes in representative shelf (0–200 m) and upper slope (200–1000 m) environments for the observed range of O_{2BW} (1–200 μM) and compare these to the measured data in Figure 1. Water depths of 100 m and 600 m (respectively) were chosen based on conventional hypsometric intervals [*Menard and Smith*, 1966]. In the model, solids are transported dynamically by sediment accumulation and by bioturbation in the upper mixed surface layer where metazoans mainly reside. Solutes are also affected by molecular diffusion and bioirrigation, the latter describing the nonlocal exchange of seawater with pore water by burrowing fauna. The model is described fully in the supporting information. It is based on previous empirical diagenetic models, and for greater transparency we have formulated the biogeochemical reactions and parameters in line with these studies [e.g., *Van Cappellen and Wang*, 1996; *Wang and Van Cappellen*, 1996; *Berg et al.*, 2003; *Dale et al.*, 2009, 2013].

Table 2. Key Model Parameters Used in the Simulation of the Shelf and Slope Sediments[a]

	Shelf	Slope	Source
Representative water depth (m)[b]	100	600	*Menard and Smith* [1966]
Temperature of the bottom water (°C)	10	8	*Thullner et al.* [2009]
Sediment accumulation rate, ω_{acc} (cm kyr^{-1})	100	16	*Burwicz et al.* [2011]
POC rain rate, F_{POC} (mmol m^{-2} d^{-1})[c]	9.4	3	*Burdige* [2007]
Total iron oxide (Fe_T) rain rate, F_{FeT} (μmol m^{-2} d^{-1})[d]	1840	290	This study
Dissolved oxygen concentration in seawater, O_{2BW} (μM)[e]	Variable	Variable	This study
Dissolved ferrous iron concentration in seawater	0	0	This study
Rate constant for aerobic Fe^{2+} oxidation, k_{13} (M^{-1} yr)[f]	5×10^{-8}	5×10^{-8}	Various
Bioturbation coefficient at surface, $D_b(0)$ (cm^2 yr^{-1})[g]	$28\cdot f$	$18\cdot f$	*Middelburg et al.* [1997]
Bioturbation halving depth, z_{bt} (cm^2 yr^{-1})	3	3	*Teal et al.* [2008]
Bioirrigation coefficient at surface, $\alpha(0)$ (yr^{-1})[g,h]	$465\cdot f$	$114\cdot f$	*Meile and Van Cappellen* [2003]
Bioirrigation attenuation coefficient, z_{bio} (cm)[i]	2	0.75	This study
Average lifetime of the reactive POC components, a (yr)[j]	3×10^{-4}	3×10^{-4}	*Boudreau et al.* [2008]
Shape of gamma distribution for POC mineralization, υ (–)[j]	0.125	0.125	*Boudreau et al.* [2008]

[a]The complete model is described in the supporting information.
[b]The mid-depth of the shelf (0–200 m) and upper slope (200–1000 m) according to *Menard and Smith* [1966].
[c]Table 4 in *Burdige* [2007], based on his compilation of benthic carbon oxidation rates.
[d]Fluxes of total particulate iron oxide (Fe_T) to the sediment were based on the Fe content in average sedimentary rock (~5%) [*Garrels and Mackenzie*, 1971] which is similar to Fe content in red clays [*Glasby*, 2006]. The total Fe flux was calculated using the equation $0.05\cdot\omega_{acc}\cdot(1-\varphi(L))\cdot\rho_s/A_W$ where $\varphi(L)$ is the porosity of compacted sediment (0.7), ρ_s is the dry sediment density (2.5 g cm^{-3}), and A_W is the standard atomic weight of iron (55.8 g mol^{-1}). Fifty percent of this flux is unreactive [*Poulton and Raiswell*, 2002], and the other 50% is divided equally among Fe_{HR}, Fe_{MR}, and Fe_{PR} (see text).
[e]Values tested in the model are 1, 2, 5, 10, 15, 25, 50, 100, and 200 μM.
[f]*Van Cappellen and Wang* [1996], *Wang and Van Cappellen* [1996], *Berg et al.* [2003], and others. See supporting information for reaction stoichiometry and kinetics.
[g]A dimensionless factor that scales the bioturbation and bioirrigation coefficients to O_{2BW} (μM) is *f*. It is equal to $0.5+0.5\cdot\mathrm{erf}((O_{2BW}-a)/b)$, where erf is the error function and *a* (20 μM) and *b* (12 μM) are constants that define the steepness of decline of *f* with decreasing O_{2BW}.
[h]*Meile and Van Cappellen* [2003] calculated the average bioirrigation coefficient in surface sediments ($\overline{\alpha}$, year^{-1}) based on total sediment oxygen uptake and bottom water O_2. As a first approximation, sediment oxygen uptake was assumed to be equal to F_{POC}. $\alpha(0)$ was calculated from $\overline{\alpha}$ following *Thullner et al.* [2009] for a bottom water O_2 concentration of 120 μM which is representative of shelf and slope environments. Irrigation of Fe^{2+} was scaled to 20% of that for the other solutes due to its high affinity for oxidation on burrow walls.
[i]The depth of the sediment affected by irrigation on the shelf was adjusted to coincide with the depth of the bioturbation zone (approximately 7 cm).
[j]A full description of POC degradation kinetics is given in the supporting information.

The parameterization of key transport processes, boundary conditions, and kinetic parameters was achieved using global empirical relationships where possible (Table 2). The sedimentation rate and surface bioturbation coefficient were calculated on the basis of water depth [*Burwicz et al.*, 2011; *Middelburg et al.*, 1997]. Similarly, *Burdige* [2007] compiled a database of sediment C_{OX} for the same water depth intervals as used here. As a first approximation, this was assumed to be equal to the total rain rate of particulate organic carbon (POC) to the seafloor since less than 10% of organic matter reaching the ocean floor is ultimately preserved in marine sediments [*Hedges and Keil*, 1995]. Bioirrigation coefficients were calculated following the procedure of *Meile and Van Cappellen* [2003]. In line with other models, irrigation of Fe^{2+} was lowered relative to other solutes due to its high affinity to oxidation on burrow walls [*Berg et al.*, 2003; *Dale et al.*, 2013]. Fluxes of total iron oxides were defined according to the bulk sedimentation rate (Table 2).

Due to the general scarcity of data from sediments underlying oxygen-deficient waters, these global relationships apply to normal oxic conditions. Yet the bioirrigation and bioturbation coefficients cannot be treated as constant parameters in the simulations due to the dependency of metazoans on oxygen. Faunal activity levels under low O_2 are not well documented, but the rate and intensity of bioturbation and irrigation are probably lower [*Diaz and Rosenberg*, 1995; *Middelburg and Levin*, 2009]. The bioirrigation and bioturbation coefficients were thus multiplied by a factor (*f*) that mimics the reduction in faunal activity at low O_{2BW} (Table 2). Specifically, the maximum bioirrigation and bioturbation rates are reduced by 50% when O_{2BW} is at the level where shifts in faunal community structure occur (approximately 20 μM) [*Levin and Gage*, 1998]. Bioirrigation and bioturbation rates are depressed even further at lower O_{2BW}, in line with field observations [*Dale et al.*, 2013]. The model sensitivity to constant animal mixing rates for all O_{2BW} levels is shown below.

Continuum kinetics for describing POC degradation is a key aspect of the model [*Middelburg*, 1989; *Boudreau and Ruddick*, 1991]. This approach captures the temporal evolution of organic matter reactivity, as opposed to multi-G models that predefine a fixed first-order decay constant of one or more carbon fractions [*Westrich and Berner*, 1984]. However, continuum models cannot be readily applied to bioturbated sediments due to random mixing of particles of different ages by animals [*Boudreau and Ruddick*, 1991]. Thus, we developed a procedure for approximating the continuum model in bioturbated sediments by defining multiple (14) carbon pools based on the initial distribution of carbon reactivity (see supporting information). This distribution is defined by two parameters: the average lifetime of the reactive components, a (yr), and the distribution of POC reactivity, υ $(-)$ (Table 2). Low υ values indicate that organic matter is dominated by refractory components, whereas higher values correspond to a more even distribution of reactive types. Similarly, organic matter characterized by low a will be rapidly degraded below the sediment-water interface, whereas a high a implies less reactive material that is more likely to be buried to deeper sediments. While we can expect some regional differences in these parameters, we used values corresponding to fresh organic matter to shelf and slope settings [*Boudreau et al*., 2008]. This is a reasonable, but not entirely robust, assumption given relatively rapid particulate sinking rates in the water column [*Kriest and Oschlies*, 2008].

A comprehensive iron cycle is included. The reactivity of particulate iron (oxyhydr)oxides (hereafter Fe oxides) was defined according to the widely employed classification based on wet chemical extraction methods [*Canfield et al*., 1992; *Raiswell and Canfield*, 1998; *Poulton et al*., 2004]. Reactive Fe oxides can be broadly defined as highly reactive (Fe_{HR}), moderately reactive (Fe_{MR}), or poorly reactive (Fe_{PR}). Fe_{HR} has a half-life of <1 yr and represents iron contained within amorphous and reactive crystalline oxides (ferrihydrite, goethite, lepidocrocite, and hematite), pyrite, and acid volatile sulfides, plus a small fraction of iron in reactive silicates [*Canfield et al*., 1992; *Raiswell and Canfield*, 1998]. Fe_{PR} has a half-life of at least 10^5 years and represents iron released from a wide range of reactive silicates and magnetite. Fe_{MR} comprises all the iron with a reactivity intermediate between Fe_{HR} and Fe_{PR} (i.e., magnetite and reactive silicates) with a half-life of 10^2 years. An additional terrigenous detrital iron fraction, representing Fe bound within silicate minerals (Fe_U), is essentially unreactive on early diagenetic time scales and constitutes about half of all sedimentary iron underlying oxic waters [*Poulton and Raiswell*, 2002]. The model simulates all four of these fractions, defined chemically as $Fe(OH)_3$.

The Fe cycle involves a number of oxidation-reduction pathways (see supporting information). These include authigenic precipitation of Fe_{HR} via aerobic and anaerobic oxidation of ferrous iron; processes that constitute an efficient geochemical barrier against DFe release from the sediment [*McManus et al*., 1997; *Berg et al*., 2003]. Reactive Fe oxides can be reduced by dissolved sulfide according to the reaction kinetics proposed by *Poulton et al*. [2004]. Fe_{HR} is also consumed by dissimilatory iron reduction (DIR), whereas the other phases are too crystalline (unreactive) to be of benefit to iron-reducing bacteria [*Weber et al*., 2006]. Nonreductive dissolution of iron has also been proposed to be a dominant source of benthic iron on continental margins that display low rates of reductive Fe dissolution [*Radic et al*., 2011; *Jeandel et al*., 2011; *Homoky et al*., 2013; *Conway and John*, 2014]. However, this process has not been described mechanistically and is not considered in our model at this point in time. Fe_{HR} further undergoes aging into more crystalline Fe_{MR} [*Cornell and Schwertmann*, 1996]. The iron module also includes iron monosulfide (FeS) and pyrite (FeS_2) precipitation, the latter via the H_2S pathway (Berzelius reaction) and by reaction with elemental sulfur, S^0 (Bunsen reaction) [*Rickard and Luther*, 2007]. FeS and FeS_2 can be oxidized aerobically, whereas S^0 can disproportionate to sulfate and sulfide.

The model was coded and solved using the method of lines with MATHEMATICA 7.0 assuming a diffusive boundary layer of 0.04 cm thickness at the sediment-water interface [*Boudreau*, 1996]. Further details on the model solution can be found in the supporting information.

4. Model Results

The model reproduces the trend of higher DFe fluxes with decreasing O_{2BW} (Figure 1a) and increasing C_{OX} (Figure 1b). The absolute magnitude of the modeled fluxes for the shelf and slope settings depends on the water depths chosen to represent these environments, meaning that the fluxes are not as rigidly defined as implied in the plots. The modeled DFe fluxes for each O_{2BW} interval in the anoxic and severely hypoxic intervals are underestimated. Yet with the exception of the anoxic shelf, removing the four fluxes

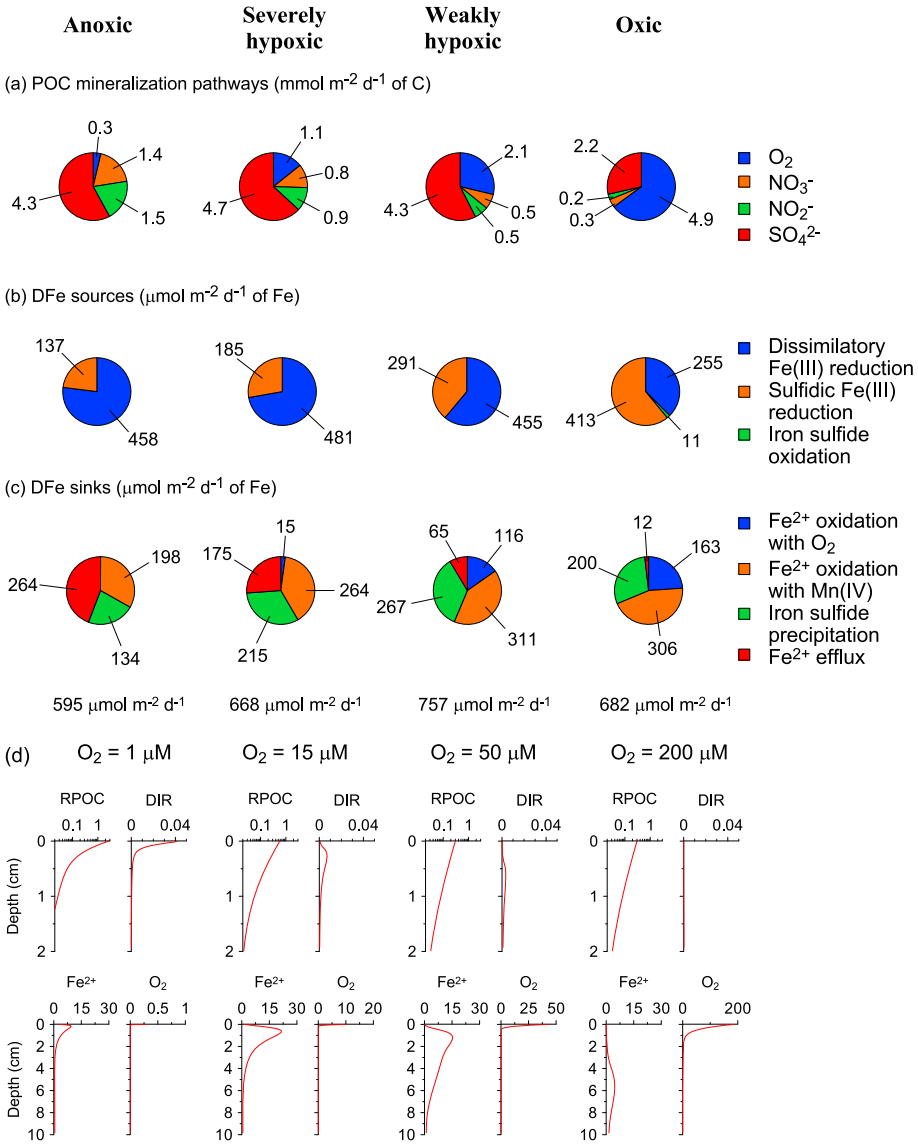

Figure 2. Simulated rates for the shelf environment for each oxygen regime are indicated at the top of the figure (Figures 2a–2c). (a) POC mineralization pathways. Fe and Mn oxide reduction rates are <0.1 mmol m^{-2} d^{-1} and not indicated. (b) DFe sources. Iron sulfide oxidation is negligible and only shown for the oxic setting. (c) DFe sinks. Oxidation by NO_3^- and irrigation are negligible and not shown. Aerobic oxidation of ferrous iron in the anoxic setting is zero and also not shown. The total sum of sinks (= sum of sources) is shown underneath the lower pie charts. (d) Sediment depth profiles of POC mineralization rate (RPOC) and dissimilatory iron reduction (DIR) in mmol cm^{-3} yr^{-1} of C and dissolved ferrous iron and oxygen concentration in μM for representative O_{2BW} in each interval (note different depth scales). Total fluxes on the slope are lower, but the pathways are qualitatively similar.

>300 μmol m^{-2} d^{-1} improves the agreement with the model (open symbols, Figure 1a). The anoxic shelf flux is tenuous because only two data points are available here.

As O_{2BW} increases, a larger fraction of POC is respired by O_2 at the expense of other electron acceptors, principally sulfate (Figure 2a). DIR accounts for less than 2% of POC respiration under all O_{2BW} conditions on the shelf and less than 0.2% on the slope. Nonetheless, DIR constitutes the largest source of DFe for anoxic and hypoxic settings (Figure 2b). At higher O_{2BW}, reduction of iron oxides by sulfide becomes more important. This finding is counterintuitive because sulfidic reduction is expected to be less pronounced as O_{2BW} increases. It can be explained by the increase in bioturbation which mixes labile iron oxide below the surface sediment where POC mineralization rates are highest (Figure 2d). This results in a less pronounced

Table 3. Input Parameters and Boundary Conditions Used in the Standard Model and for the Sensitivity Analysis[a]

	Standard Model	Sensitivity Analysis
Representative water depth (m)	350	350
Sediment accumulation rate, ω_{acc} (cm kyr^{-1})	60	60
POC rain rate, F_{POC} (mmol m^{-2} d^{-1})	6.2	0.5–15[b]
Total iron oxide (Fe_T) rain rate, F_{FeT} (μmol m^{-2} d^{-1})	1110	1110
Dissolved oxygen concentration in seawater, O_{2BW} (μM)	120	1–200[c]
Bioturbation coefficient at surface, $D_b(0)$ (cm^2 yr^{-1})	$23 \cdot f$	$23 \cdot f$
Bioirrigation coefficient at surface, $\alpha(0)$ (year^{-1})	$290 \cdot f$	$290 \cdot f$
Bioirrigation attenuation coefficient, z_{bio} (cm)	1.4	1.4

[a]Model parameters that are unchanged from Table 2 are not listed.
[b]Values tested (in mmol m^{-2} d^{-1}) are 0.5, 1, 2, 4, 6, 8, 10, 12, 14, and 16, which are equivalent to C_{OX} of 0.4, 0.8, 1.7, 3.3, 5.0, 6.6, 8.3, 9.9, 11.6, and 13.2.
[c]Values tested are 1, 2, 5, 10, 15, 25, 50, 100, and 200 μM.

DIR peak and a greater likelihood that iron oxide is instead reduced by sulfide deeper down. In these subsurface horizons, iron undergoes repeated redox cycling (Figures 2b and 2c) whereby DFe is oxidized to Fe(III), mainly by Mn(IV), and then regenerated when the authigenic iron oxide is again reduced by sulfide or organic matter [e.g., *Wang and Van Cappellen*, 1996]. This tends to increase the apparent total rate of iron sources (or sinks), from 595 μmol m^{-2} d^{-1} under anoxia to 757 μmol m^{-2} d^{-1} under weakly hypoxic conditions, even though the total flux of particulate iron to the sediment is the same in all cases.

Under near-anoxic conditions, almost half of all DFe is lost to the water column (Figure 2c). A sink switching effect takes place with higher O_{2BW}, whereby DFe oxidation increases at the expense of benthic DFe loss, thereby leading to greater retention of DFe. DFe fluxes fall sharply when bottom waters transition from severe to weak hypoxia, which is reflected in the field observations by the increase in DFe fluxes when $O_{2BW} < 20$ μM (Figure 1). This concentration may represent a tipping point, beyond which sediments become highly efficient at retaining the iron deposited on the sediment surface. In this regard, it is noteworthy that the boundary between surface sediments that are enriched and depleted in Fe in the Peruvian oxygen minimum zone is located exactly where bottom oxygen concentrations rise above 20 μM [*Scholz et al*., 2014a].

The impact of O_{2BW} on DFe fluxes is illustrated more graphically by the DFe pore water concentrations in Figure 2d. Under very low O_{2BW}, the DFe concentration gradient at the sediment-water interface is extremely sharp, which drives a large flux across the diffusive boundary layer. In this case, O_2 barely penetrates the sediment and acts as a poor geochemical barrier to DFe flux [*McManus et al*., 1997]. Under weakly hypoxic conditions, O_{2BW} penetrates deeper leading to a more efficient oxidative sink for DFe. The resulting DFe concentration gradient in the uppermost millimeters is markedly shallower and the flux to the bottom water much smaller. Finally, under normal oxic conditions, the DFe peak is spatially separated from the surface by several centimeters and only a very weak DFe flux is predicted.

We propose that the DFe flux tipping point is related to sediment ventilation by burrowing animals. The impact of irrigation in our model is demonstrated by the dashed curves in Figure 1a which show that DFe fluxes are much lower on the shelf and slope if faunal activity is unaffected by low O_{2BW}. This conflicts with *Elrod et al*. [2004], who suggested that DFe fluxes were enhanced by bioirrigation in Monterey Bay sediments ($O_{2BW} > 100$ μM). Yet the importance of bioirrigation in mitigating DFe fluxes is supported by previous observations. First, mesocosm experiments showed that burrowing fauna increase iron retention due to rapid immobilization of DFe as particulate iron oxide phases on burrow walls [*Lewandowski et al*., 2007]. These results have been reproduced using bioirrigation models that employ empirically derived rate constants for aerobic DFe oxidation [*Meile et al*., 2005]. Second, bottom water DFe concentrations in the later stages of sediment incubations increase quasi-exponentially concomitant with dissolved oxygen depletion [*Severmann et al*., 2010]. This has been attributed to the loss of the surface oxidized layer on the walls of animal burrows as well as a reduced rate of DFe oxidation in oxygen-depleted chamber waters. More generally, DFe fluxes are low in sediments bearing a surface oxidized layer [*McManus et al*., 1997]. Clearly, then, in addition to C_{OX}, DFe fluxes show a strong dependence on O_{2BW}, especially for concentrations below 20 μM. In the following section, we derive a function based on both these variables to predict DFe fluxes from sediments.

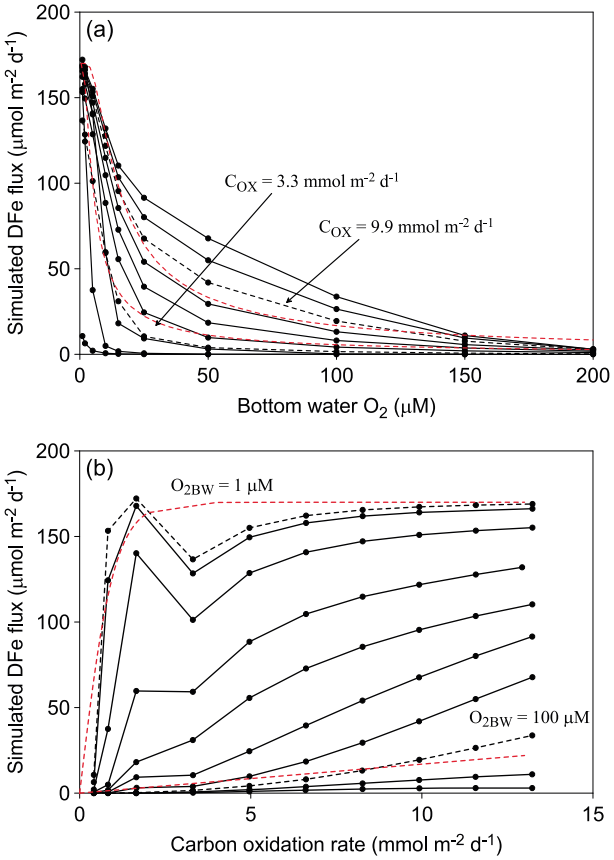

Figure 3. Simulated DFe fluxes from the standardized numerical model versus (a) bottom water oxygen concentration and (b) carbon oxidation rate. In Figure 3a, the results for a C_{OX} of 9.9 and 3.3 mmol m^{-2} d^{-1} are shown as dashed curves and compared to the predicted fluxes from the new function (equation (1)) in adjacent red dashed curves. In Figure 3b, the results for O_{2BW} of 1 and 100 μM are compared to the new function. All other black curves correspond to the O_{2BW} and C_{OX} intervals listed in Table 3.

5. Derivation of a Predictive Function for Benthic Iron Fluxes

An empirical function for predicting benthic DFe fluxes from C_{OX} and O_{2BW} was derived using a more detailed sensitivity analysis. This was based on a standardized model defined by the average parameter values of the shelf and slope settings (Table 3). A series of model runs was executed where organic matter rain rate and O_{2BW} were varied between 0.5–16 mmol m^{-2} d^{-1} and 1–200 μM, respectively. The corresponding C_{OX} for these rain rates is 0.4–13.2 mmol m^{-2} d^{-1}. These ranges are characteristic of the sites in Table 1 and much of the seafloor in general. Although rain rate and O_{2BW} were the only two model aspects to be varied directly, the bioturbation and bioirrigation coefficients were dependent on O_{2BW}, as described previously. This avoids anomalous scenarios, such as high bioirrigation at sites with low benthic respiration.

The dependence of DFe flux on O_{2BW} for constant values of C_{OX} is shown in Figure 3a. DFe flux increases with decreasing O_{2BW} for all C_{OX}, with a tipping point centered at around 20 μM, as observed previously. Furthermore, sediments release more iron as C_{OX} increases due to higher rates of aerobic carbon respiration at the expense of DFe oxidation. Benthic DFe flux also responds strongly to small increases in C_{OX} when O_{2BW} is below approximately 10 μM (Figure 3b). The pronounced peak in DFe centered at C_{OX} = 2 mmol m^{-2} d^{-1} originates from high DIR rates close to the sediment surface (cf. Figure 2d). The subsequent dip in DFe flux when C_{OX} ~ 4 mmol m^{-2} d^{-1} signifies sequestration of iron into sulfide minerals as sulfate reduction rates increase. DFe fluxes then gradually increase again with higher C_{OX} as in Figure 3a. These results demonstrate that C_{OX} is itself an important factor to consider for predicting DFe fluxes, in addition to the total flux of labile particulate iron (see below).

The sensitivity analysis supports observations that C_{OX} acts on DFe flux in an opposite way to O_{2BW} [*Elrod et al.*, 2004; *Severmann et al.*, 2010]. Hence, we derived a predictive function for DFe fluxes (in μmol m^{-2} d^{-1}) to reflect this behavior:

$$\text{DFe flux} = \gamma \cdot \tanh\left(\frac{C_{OX}}{O_{2BW}}\right) \quad (1)$$

where C_{OX} is in mmol m^{-2} d^{-1} and O_{2BW} is in μM. The maximum flux that can escape the sediment for a given Fe content and reactivity is γ. In our simulations, this is predicted to be 170 μmol m^{-2} d^{-1}.

The function is an example of a 0-D vertically integrated sediment model following the criteria of *Soetaert et al.* [2000]. Although the function is unable to simulate the local minimum of the DFe flux at low O_{2BW}, it broadly reproduces the hyperbolic trends in the sensitivity analysis results (dashed red curves, Figure 3). A comparison of the new function with each paired C_{OX} and O_{2BW} point on these curves shows that it

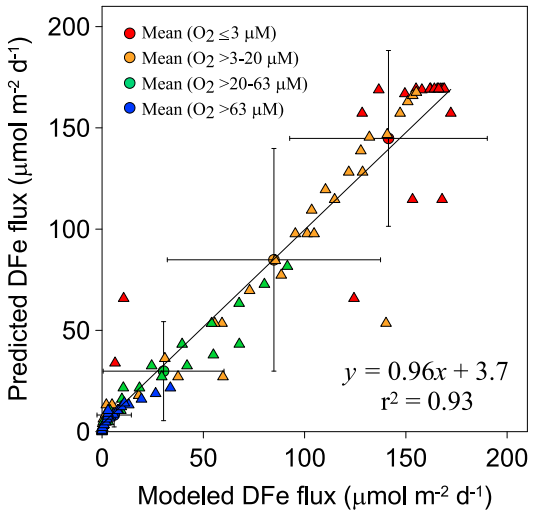

Figure 4. Comparison of the DFe fluxes simulated using the standardized numerical model for each paired O_{2BW}-C_{OX} data (black circles in Figure 3) and the DFe fluxes predicted using equation (1), color coded according to O_{2BW} (triangles). The large circles represent the mean flux ± standard deviation in each O_{2BW} interval. The straight line is the linear regression curve (equation indicated).

explains 93% of the variance in the modeled rates, with a standard error of the slope of 0.027 μmol m^{-2} d^{-1} (Figure 4). C_{OX} and O_{2BW} alone each explain less than 20%. More complex functions did not improve the fit significantly.

The extreme DFe fluxes observed on the Peruvian shelf, Californian Borderland Basins, and the Eel River mouth are not captured by the new function. One factor to consider may simply be that sediments display a wide range of reactive iron content. In our simulations we used a Fe_{HR}/Fe_T of 0.17, which is within the range of 0.08–0.40 for continental margin sediments [*Raiswell and Canfield*, 1998]. Rivers tend to deposit large amounts of terrigenous inorganic material on the shelf which may be more enriched in Fe_{HR} compared to the global average [*Poulton and Raiswell*, 2002]. We tested the sensitivity of DFe fluxes to the Fe_{HR} content by repeating the model simulations for the shelf site with 1 and 100 μM O_{2BW}. In these simulations, the total iron flux was held constant but the fluxes of Fe_{HR} and Fe_U were varied. The results show a quasi-linear dependence of benthic DFe fluxes on the Fe_{HR}/Fe_T ratio with a steeper response when O_{2BW} is in the normal oxic range compared to the anoxic range (Figure 5). The model predicts that the observed variability in Fe_{HR}/Fe_T for the Fe_T flux used in the simulations can result in DFe fluxes that vary by an order of magnitude. This supports the idea that high DFe fluxes on the Eel River shelf are driven by a higher-than-average Fe_{HR} content [*Severmann et al.*, 2010] and, possibly, seasonal variability too [*Severmann et al.*, 2010; *Berelson et al.*, 2003; *Pakhomova et al.*, 2007]. Similarly, low DFe fluxes were calculated from pore water profiles in sediments with a low Fe_{HR} content on the South African margin [*Homoky et al.*, 2013]. Clearly, though, the total Fe_{HR} flux is the controlling factor on DFe flux rather than Fe_{HR}/Fe_T, the latter of which is likely to be determined by the weathering regime rather than the overall flux of terrigenous material.

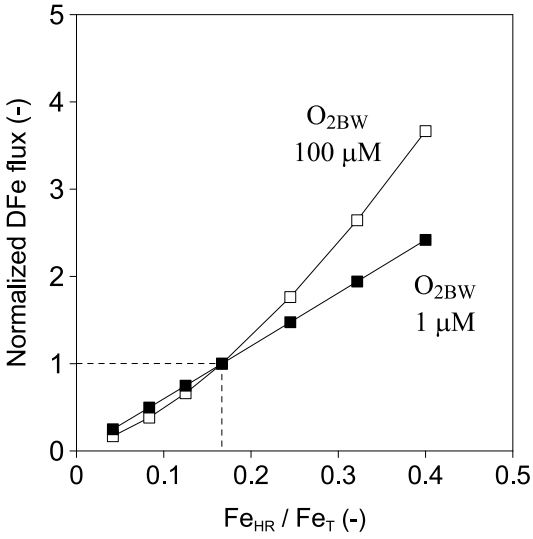

Figure 5. Sensitivity of modeled benthic DFe fluxes in shelf sediments to the Fe_{HR}/Fe_T ratio in particulate iron oxide deposited on the seafloor [*Raiswell and Canfield*, 1998]. Results are shown for low (1 μM) and high (100 μM) O_{2BW}. DFe fluxes are normalized to the modeled shelf fluxes in Figure 1a for O_{2BW} = 1 and 100 μM, indicated by the dashed lines.

By contrast, terrigenous Fe supply to the California Borderland Basins and the shallow Peruvian shelf is very low. Extremely high benthic DFe fluxes in these regions may be caused by the transient occurrence of oxidizing conditions in the bottom water and the focused discharge of DFe after the recurrence of anoxia [*Scholz et al.*, 2011; *Noffke et al.*, 2012]. The idea is that during oxic periods, a thin oxidized layer develops on the sediment surface which favors the precipitation of Fe oxides and mitigates DFe flux to the bottom water. Deposition of particulate Fe oxides from the water column would also be enhanced under these conditions. A resurgence of anoxic conditions favors reductive dissolution of the accumulated oxides, leading to pulsed release of DFe to the bottom water. Moreover, iron fluxes in

Table 4. Dissolved Iron Fluxes From Marine Sediments Calculated Using Equation (1)

	Area[a] (10^{12} m^2)	Mean C_{OX}[b] (mmol m^{-2} d^{-1})	Mean DFe Flux[c] (μmol m^{-2} d^{-1})	Total DFe Flux[d] (Gmol yr^{-1})	Total DFe Flux[e] [*Elrod et al.*, 2004] (Gmol yr^{-1})
			Continental Margin		
Shelf (0–200 m)	27.12	9.4	7.3	72.2 ± 36.1	63.3
Upper slope (>200–1000 m)	16.01	3.0	3.5	20.5 ± 10.3	11.9
Lower slope (>1000–2000 m)	15.84	1.5	2.9	16.6 ± 8.4	5.9
Total margin[f]	58.98 (0.38)	5.5	5.1 (35)	109 ± 55 (5)	81
			Deep Sea		
>2000 m	302.5	0.4	0.37	41 ± 21	30
			Global Ocean		
Σ				150 ± 75	111

[a] *Menard and Smith* [1966].
[b] *Burdige* [2007].
[c] Using the gridded O_{2BW} and bathymetry in combination with equation (1).
[d] Integrated over the corresponding ocean area. The uncertainties (±) are calculated based on the uncertainty in Fe_{HR} and Fe_T content. Standard deviations in Fe_{HR} and Fe_T are reported for a mean marine sediment by *Poulton and Raiswell* [2002, Table 7]. Using standard error propagation rules, the relative error in the Fe_{HR}/Fe_T ratio using their data is 50%, which is taken as the error in DFe flux.
[e] The flux calculated assuming the regression provided by *Elrod et al.* [2004] in Figure 1. For consistency with *Elrod et al.* [2004], we used a flux ratio of 0.68 μmol DFe/mmol carbon oxidized in this calculation, ignoring the intercept DFe flux of 0.5 μmol m^{-2} d^{-1} in their linear regression equation.
[f] Values in parenthesis correspond to sediments underlying oxygen-deficient bottom waters (<20 μM).

such temporally anoxic and occasionally euxinic settings such as the Peruvian shelf may be largely influenced by additional controls such as the availability of sulfide in the pore water and bottom water and benthic boundary layer [*Scholz et al.*, 2014b]. These factors cannot be constrained with our benthic model, as we assume a bottom water sulfide concentration of zero in all model runs. More generally, the magnitude of the terrigenous Fe_{HR} flux and/or focused deposition of Fe oxides due to seasonal or other transient effects might play a more important role in generating the observed variability in benthic DFe fluxes than implied by the model.

6. A Revised Estimate for Global Benthic Iron Flux

Our new estimate of the global benthic DFe flux is based on spatially resolved bathymetry, O_{2BW}, and C_{OX} data. Maps of bathymetry and O_{2BW} on a 1° × 1° resolution were taken from *Bohlen et al.* [2012] based on data from the World Ocean Atlas [*Garcia et al.*, 2006]. Gridded C_{OX} data are unavailable, and instead, we used average C_{OX} for several hypsometric intervals [*Burdige*, 2007]. Upscaling using the new function (equation (1)) predicts a global DFe flux of 150 ± 75 Gmol yr^{-1} (Table 4), of which 109 ± 55 Gmol yr^{-1} is contributed by continental margin sediments and 41 ± 21 Gmol yr^{-1} by the deep sea (>2000 m). The uncertainties are calculated assuming that variability in Fe_{HR}/Fe_T and Fe_T content contributes to the largest error in the model predictions (see Table 4). This is equivalent to 50% for margin and deep-sea sediments. However, it is obvious from the scatter in Figure 1 that there are other sources of variability in DFe fluxes. This is not surprising given the physical and biogeochemical heterogeneity of continental margin sediments, implying that the calculated uncertainty is a conservative estimate [*Liu et al.*, 2010].

Note that the average DFe flux from deep-sea sediments is very low (0.37 μmol m^{-2} d^{-1}) yet globally significant by virtue of the vast expanse of the ocean basins. Nonetheless, this flux is speculative because very few flux measurements have been made in the ocean basins. Sequestration of DFe in deep-sea sediments may be more efficient than predicted, especially if other DFe removal pathways currently ignored in the model are significant, such as precipitation of authigenic carbonates, phosphates, or silicates. Consequently, the data currently only support a global DFe flux of 109 Gmol yr^{-1}, but it may be higher, especially if nonreductive iron dissolution contributes significantly to the global Fe budget [*Homoky et al.*, 2013; *Conway and John*, 2014]. In fact, the Biogeochemical Elemental Cycling ocean model that is tuned to pelagic DFe distribution does consider a very low DFe flux from the lower slope and deep basins [*Moore and Braucher*, 2008].

Taking the lower global DFe flux of 109 Gmol yr^{-1}, our model suggests that two thirds (72 Gmol yr^{-1}) is contributed by shelf sediments (Table 4). This is similar to 89 Gmol yr^{-1} derived by *Elrod et al.* [2004]

assuming a mean C_{OX} of 12 mmol m^{-2} d^{-1}. Our lower shelf C_{OX} (9.4 mmol m^{-2} d^{-1}) is derived from a well-constrained empirical relationship between C_{OX} and water depth [*Burdige*, 2007]. Using Burdige's C_{OX} would decrease Elrod et al.'s shelf estimate by around one third. Importantly, however, we find that continental slope sediments are also major sources of iron to ocean bottom waters (37.1 Gmol yr^{-1}). The implication is that sedimentary DFe release has been grossly underestimated in the marine Fe budget [*Jickells et al.*, 2005; *Boyd and Ellwood*, 2010].

Our derived global flux is 3 to 14 times higher than most previous estimates (see section 1). The average DFe flux from continental margins (5.1 μmol m^{-2} d^{-1}; Table 4) is also 3 to 5 times higher than the maximum benthic DFe flux of 1–2 μmol m^{-2} d^{-1} imposed as a seafloor boundary condition in some global iron models [e.g., *Moore et al.*, 2004; *Aumont and Bopp*, 2006]. One reason for the lower flux estimates from the global approaches may be an underestimation of organic carbon rain rates [*Moore and Braucher*, 2008]. It would be interesting to compare carbon export fluxes from these models, but this datum is unfortunately seldom reported. A more important consideration is that carbon rain rates and tracer distributions are generally poorly resolved over shelf sediments in global models, meaning that the shelf DFe flux (72.2 Gmol yr^{-1}), equivalent to two thirds of the global sedimentary DFe release, is not properly accounted for. Instead, the models are tuned to the lower DFe fluxes from slope sediments. However, a fraction of the iron released from shelf sediments is not retained in coastal waters but exported offshore in both dissolved and particulate form [*Johnson et al.*, 1999; *Lam et al.*, 2006; *Lohan and Bruland*, 2008; *de Jong et al.*, 2012]. Too little export of coastal iron to the ocean basins may lead to a too strong dependence of surface iron concentrations on atmospheric iron deposition, thus influencing model sensitivity toward this source [*Moore and Braucher*, 2008; *Tagliabue et al.*, 2014].

An additional factor to consider that has been highlighted in this study is the role of bottom water oxygen concentration. Comparison of our DFe fluxes with those predicted by *Elrod et al.* [2004] using the same C_{OX} provides a broad overview of the effect of O_{2BW}. Most notably, we find that our DFe fluxes on the continental slope are 2–3 times higher than predicted by Elrod et al.'s function (Table 4). This is partly because oxygen-deficient waters of the eastern boundary upwelling systems tend to impinge on the seafloor at these depths [*Helly and Levin*, 2004]. Sediments underlying bottom waters below the 20 μM threshold are flux hot spots, releasing DFe at an average rate of 35 μmol m^{-2} d^{-1}. They account for 4% of total DFe flux on the margin despite covering <1% of the seafloor. Yet it should be noted that the relatively coarse 1° × 1° resolution does not accurately capture shallow marginal sediments. Taking a more sophisticated approach, *Helly and Levin* [2004] estimated that around 1.4×10^{12} m^2 of sediments are in contact with bottom water <22 μM, which is equivalent to 3% by area of the shelf and upper slope (0–1000 m). Our DFe flux from oxygen-deficient regions is, therefore, likely to be a minimum estimate and may be up to a factor of 3 higher.

7. Impact of Benthic Iron Release on Oceanic Dissolved Iron Distributions

The ability of our simple function to predict DFe fluxes is encouraging because it can easily be implemented in global biogeochemical models. Most models routinely simulate dissolved oxygen and organic carbon rain rates to the seafloor ($\approx C_{OX}$). Thus, it provides a straightforward tool to test how the spatial distribution of DFe in the ocean is impacted by benthic iron release.

We tested the impact of our predictive function on global iron distributions in the ocean using the University of Victoria Earth System Climate Model (UVic ESCM). This model includes a coupled physical biogeochemical ocean component with a dynamic iron cycle [*Nickelsen et al.*, 2015]. Like other global models, shelf processes are not adequately described due to the coarse spatial resolution. The model has two iron pools, dissolved and particulate, and is similar to other global iron models [e.g., *Moore and Braucher*, 2008; *Tagliabue et al.*, 2014]. Scavenging of iron from the water column by organic particles is tuned to provide a good correlation between observed and modeled surface ocean DFe distributions. The model does not include scavenging by resuspended inorganic particles. Sedimentary iron release is proportional to carbon oxidation rate (i.e., Elrod et al.'s function), and the model further uses a simple oxygen-dependent switch threshold of 5 μM. If bottom water O_2 falls below this value, all iron deposited on the seafloor is released back to the water column. Benthic DFe fluxes predicted by the UVic ESCM model are shown in Figure 6a, and tuning of scavenging rates leads to a good fit to observed surface DFe concentrations (Figure 6b). The global benthic DFe flux predicted by the model in this configuration is 19 Gmol yr^{-1} [*Nickelsen et al.*, 2015].

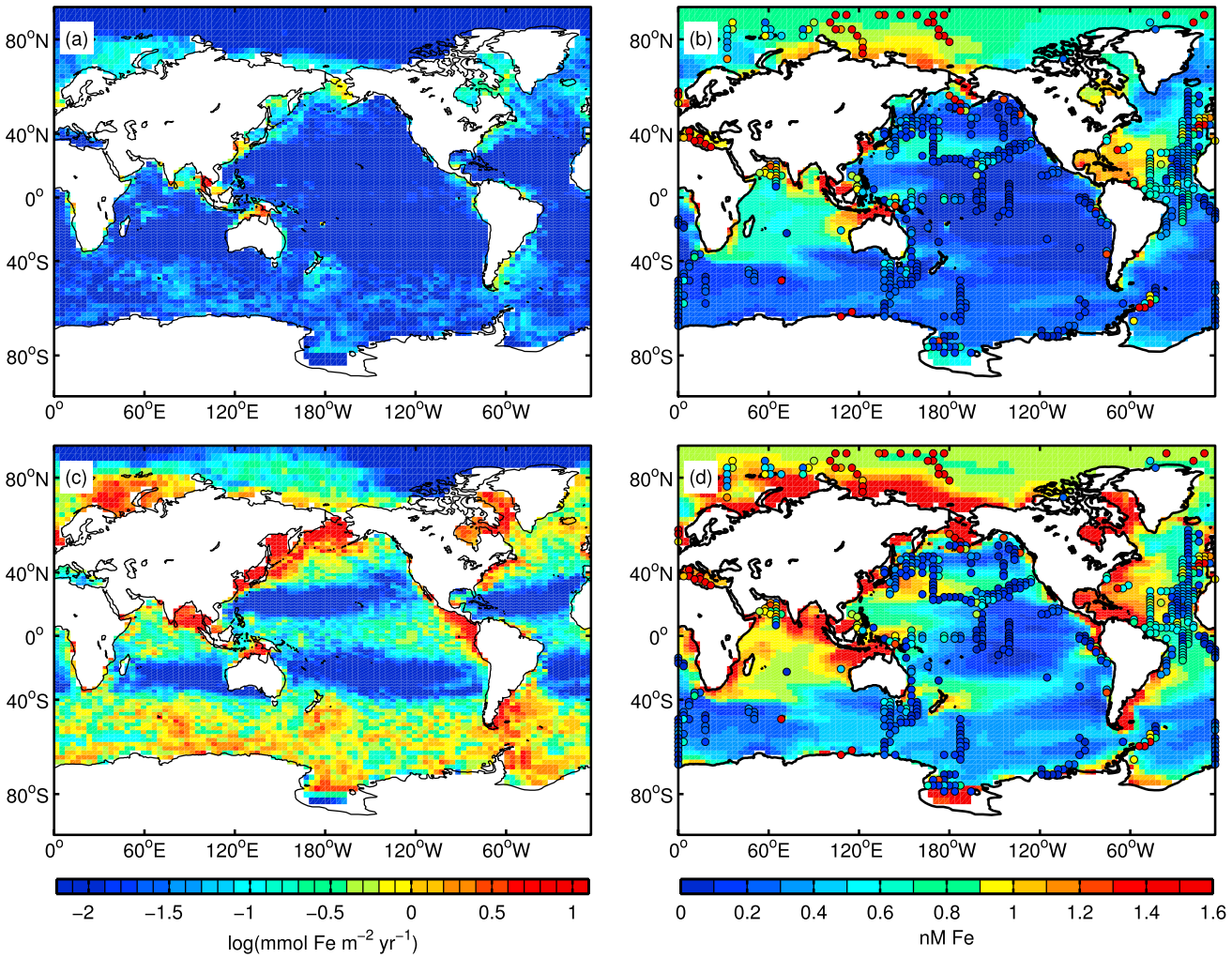

Figure 6. (a) Benthic DFe fluxes (mmol m^{-2} yr^{-1}, log scale) and (b) surface ocean DFe distributions (nM) using the UVic ESCM model [from *Nickelsen et al.*, 2015]. The results show the best model fit to observations (colored circles) [*Tagliabue et al.*, 2012]. (c and d) The model results where the new function for benthic DFe flux (equation (1)) is used to parameterize the benthic DFe flux, with all other model parameters held constant.

Benthic DFe fluxes increase strongly in the northern and eastern tropical Pacific, the Southern Ocean, and the North Atlantic when the model is executed using our function with all other parameters held constant (Figure 6c). The global DFe flux from sediments increases to 333 Gmol yr^{-1}, which is a factor of 2–3 higher than the predicted flux from the gridded data (Table 4). The elevated iron flux is caused by a positive feedback with POC rain rate to the seafloor driven by benthic Fe fertilization. Benthic DFe fluxes are thus enhanced in the new function configuration in otherwise iron-limited areas. Although scavenging depletes a fraction of the DFe released from the sediments, surface iron concentrations generally show a poorer agreement with the observations (Figure 6d). DFe concentrations are also elevated in deep waters (>3000 m) by around 0.3 nM compared to observations (not shown). This model configuration would require much higher scavenging rates in order to bring the model predictions back in line with the observations. They would need to be 4 times higher to reduce the globally averaged surface iron concentration from 0.83 nM to 0.48 nM, similar to previous "best fit" values of 0.41 nM (Figure 6b).

The sensitivity of surface ocean DFe to benthic iron release suggests that the poorly constrained scavenging rates are currently too low in the state-of-the-art global iron models. DFe removal into organic/inorganic particulates or colloids very likely prevents a large fraction of sedimentary iron reaching the surface ocean in a bioavailable form [*Honeyman et al.*, 1988; *Homoky et al.*, 2012; *John et al.*, 2012]. However, the model cannot currently resolve whether iron scavenging occurs close to the sediments or higher up in the water

column. In reality, scavenging by inorganic particles is likely to be exacerbated in intermediate and bottom nepheloid layers on continental margins [*Jahnke et al*., 1990; *Inthorn et al*., 2006]. In agreement with this, lateral relocation of sediment-derived Fe on the Peruvian margin appears to take place in colloids or nanoparticulates near the seafloor [*Scholz et al*., 2011]. A fraction of iron scavenged within these layers may be exported offshore to distant Fe-limited regions, redeposited on the seafloor or upwelled into surface waters [*Johnson et al*., 1999; *Lam et al*., 2006]. Particle settling of inorganically bound iron in addition to colloidal aggregation and pumping [*Honeyman and Santschi*, 1991] may be an important yet overlooked component of the marine Fe budget. It is worth noting that organically bound iron exported from the surface ocean to the sediments would support $<5\%$ of the measured DFe flux from the continental margins, given the C_{OX} rate in Table 4 and a molar Fe/C_{org} ratio of 20 μmol/mol [*Wu and Boyle*, 2002; *Moore and Braucher*, 2008].

We thus propose that there exists a rapid removal of benthic-derived DFe into colloidal or inorganic phases close to the seafloor in particle-rich water layers. This serves as a barrier for sedimentary DFe reaching the surface mixed layer. Given that our benthic DFe fluxes are several fold higher than those presently used in global iron models tuned to DFe distributions, the fraction of bioavailable iron that arrives at the sunlit ocean is probably much smaller than the fraction that is scavenged. Diagenetic alteration and dissolution of iron particles and aggregates following deposition on the sediment allows DFe to be returned to the water column and rescavenged. We believe that this cycle could be an important vector for transporting iron offshore away from the margins. Future studies should try to quantify these sources and sinks with the aim to improve the conceptual iron cycle in Earth system models.

8. Conclusions

The main objective of this study was to develop a simple, mathematical tool for predicting the flux of dissolved iron (DFe) from marine sediments and to better quantify its contribution to the global iron cycle. We derived an empirical function that unifies the role of bottom water oxygen concentration (O_{2BW}) and organic carbon oxidation rate in sediments (C_{OX}) as key controls on benthic DFe flux. The new function predicts a global DFe flux that is around 5 times higher than the previous estimates derived using global models. This can be attributed to (i) inadequate treatment of the role of O_2 on benthic DFe fluxes in global models and (ii) poorly resolved biogeochemical dynamics on the shelf (for the sake of computational efficiency) where two thirds of the global sedimentary DFe release occurs.

When the new function is applied to the state-of-the-art intermediate-complexity Earth system climate model UVic ESCM [*Nickelsen et al*., 2015], simulated surface water DFe concentrations are increased significantly over most of the ocean. This leads us to conclude that iron scavenging rates, mainly as inorganic particulates and colloidal aggregates close to the seafloor, must also be far higher than assumed previously. Otherwise, a strong positive feedback becomes established between primary productivity (hence C_{OX}) and DFe flux. The enhanced benthic DFe source may not have critical consequences for the current generation of ocean models if they correctly simulate the net flux of sediment iron that reaches the surface. However, the excess benthic iron that is scavenged close to the seabed is likely to be poorly represented. This could have important implications for the marine Fe budget as well as for simulating long-range transport of iron to Fe-limited regions. Once the significance of this "dark" Fe cycle has been evaluated and parameterized more carefully, it would be interesting to test whether simulated atmospheric CO_2 concentrations during the Last Glacial Maximum are greatly diminished in global model simulations that employ our new benthic Fe input function [e.g., *Parekh et al*., 2006].

Acknowledgments
We thank the editorial team and two anonymous reviewers for their thoughtful comments. This work is a contribution of the Sonderforschungsbereich 754 "Climate-Biogeochemistry Interactions in the Tropical Ocean" (www.sfb754.de) financially supported by the Deutsche Forschungsgemeinschaft (DFG). The Seventh Framework Program of the European Union supported the participation of F.S. (Marie Curie IOF 300648, BICYCLE). All field data used in this manuscript have been published previously and are directly obtainable from the literature cited in Table 1.

References

Andersson, J. H., J. W. M. Wijsman, P. M. J. Herman, J. J. Middelburg, K. Soetaert, and C. Heip (2004), Respiration patterns in the deep ocean, *Geophys. Res. Lett.*, *31*, L03304, doi:10.1029/2003GL018756.

Archer, D. E., and K. Johnson (2000), A model of the iron cycle in the ocean, *Global Biogeochem. Cycles*, *14*, 269–279, doi:10.1029/1999GB900053.

Aumont, O., and L. Bopp (2006), Globalizing results from ocean in situ iron fertilization studies, *Global Biogeochem. Cycles*, *20*, GB2017, doi:10.1029/2005GB002591.

Aumont, O., E. Maier-Reimer, S. Blain, and P. Monfray (2003), An ecosystem model of the global ocean including Fe, Si, P colimitations, *Global Biogeochem. Cycles*, *17*(2), 1060, doi:10.1029/2001GB001745.

Berelson, W. M., J. McManus, K. Coale, K. Johnson, D. Burdige, T. Kilgore, D. Colodner, F. Chavez, R. Kudela, and H. Boucher (2003), A time series of benthic flux measurements from Monterey Bay, CA, *Cont. Shelf Res.*, *23*, 457–481.

Berg, P., S. Rysgaard, and B. Thamdrup (2003), Dynamic modeling of early diagenesis and nutrient cycling. A case study in an Arctic marine sediment, *Am. J. Sci.*, *303*, 905–955.
Bohlen, L., A. W. Dale, S. Sommer, T. Mosch, C. Hensen, A. Noffke, F. Scholz, and K. Wallmann (2011), Benthic nitrogen cycling traversing the Peruvian oxygen minimum zone, *Geochim. Cosmochim. Acta*, *75*, 6094–6111.
Bohlen, L., A. W. Dale, and K. Wallmann (2012), Simple transfer functions for calculating benthic fixed nitrogen losses and C:N:P regeneration ratios in global biogeochemical models, *Global Biogeochem. Cycles*, *26*, GB3029, doi:10.1029/2011GB004198.
Boudreau, B. P. (1996), A method-of-lines code for carbon and nutrient diagenesis in aquatic sediments, *Comput. Geosci.*, *22*, 479–496.
Boudreau, B. P., and B. R. Ruddick (1991), On a reactive continuum representation of organic matter diagenesis, *Am. J. Sci.*, *291*, 507–538.
Boudreau, B. P., C. Arnosti, B. B. Jørgensen, and D. E. Canfield (2008), Comment on "Physical model for the decay and preservation of marine organic carbon", *Science*, *319*, 1616–1617.
Boyd, P. W., and M. J. Ellwood (2010), The biogeochemical cycle of iron in the ocean, *Nat. Geosci.*, *3*, 675–682.
Burdige, D. J. (2007), Preservation of organic matter in marine sediments: Controls, mechanisms, and an imbalance in sediment organic carbon budgets?, *Chem. Rev.*, *107*, 467–485.
Burwicz, E. B., L. H. Rüpke, and K. Wallmann (2011), Estimation of the global amount of submarine gas hydrates formed via microbial methane formation based on numerical reaction-transport modeling and a novel parameterization of Holocene sedimentation, *Geochim. Cosmochim. Acta*, *75*, 4562–4576.
Canfield, D. E., R. Raiswell, and S. Bottrell (1992), The reactivity of sedimentary iron minerals toward sulfide, *Am. J. Sci.*, *292*, 659–683.
Conway, T. M., and S. G. John (2014), Quantification of dissolved iron sources to the North Atlantic Ocean, *Nature*, *511*, 212–215.
Cornell, R. M., and U. Schwertmann (1996), *The Iron Oxides: Structure, Properties, Reactions, Occurrences and Uses*, 703 pp., Wiley-VCH, Darmstadt, Germany.
Cullen, J. T., M. Chong, and D. Ianson (2009), British Columbian continental shelf as a source of dissolved iron to the subarctic northeast Pacific Ocean, *Global Biogeochem. Cycles*, *23*, GB4012, doi:10.1029/2008GB003326.
Dale, A. W., V. Brüchert, M. Alperin, and P. Regnier (2009), An integrated sulfur isotope model for Namibian shelf sediments, *Geochim. Cosmochim. Acta*, *73*, 1924–1944.
Dale, A. W., V. J. Bertics, T. Treude, S. Sommer, and K. Wallmann (2013), Modeling benthic–pelagic nutrient exchange processes and pore water distributions in a seasonally hypoxic sediment: Evidence for massive phosphate release by *Beggiatoa*?, *Biogeosciences*, *10*, 629–651, doi:10.5194/bg-10-629-2013.
de Jong, J., V. Schoemann, D. Lannuzel, P. Croot, H. de Baar, and J. -L. Tison (2012), Natural iron fertilization of the Atlantic sector of the Southern Ocean by continental shelf sources of the Antarctic Peninsula, *J. Geophys. Res.*, *117*, G01029, doi:10.1029/2011JG001679.
Diaz, R. J., and R. Rosenberg (1995), Marine benthic hypoxia—Review of ecological effects and behavioral responses on macrofauna, *Oceanogr. Mar. Biol.*, *33*, 245–303.
Elrod, V. A., W. M. Berelson, K. H. Coale, and K. S. Johnson (2004), The flux of iron from continental shelf sediments: A missing source for global budgets, *Geophys. Res. Lett.*, *31*, L12307, doi:10.1029/2004GL020216.
Friedrich, J., C. Dinkel, G. Friedl, N. Pimenov, J. Wijsman, M. T. Gomoiu, A. Cociasu, L. Popa, and B. Wehrli (2002), Benthic nutrient cycling and diagenetic pathways in the North-western Black Sea, *Estuarine Coastal Shelf Sci.*, *54*, 369–383.
Galbraith, E. D., A. Gnanadesikan, J. P. Dunne, and M. R. Hiscock (2010), Regional impacts of iron-light colimitation in a global biogeochemical model, *Biogeosciences*, *7*, 1043–1064.
Garcia, H. E., R. A. Locarnini, T. P. Boyer, and J. I. Antonov (2006), *World Ocean Atlas 2005, Volume 3: Dissolved Oxygen, Apparent Oxygen Utilization, and Oxygen Saturation*, *NOAA Atlas NESDIS*, vol. 63, edited by S. Levitus, 342 pp., NOAA, Silver Spring, Md.
Garrels, R. M., and F. T. Mackenzie (1971), *Evolution of Sedimentary Rocks*, 397 pp., Norton, New York.
Glasby, G. P. (2006), Manganese: Predominant role of nodules and crusts, in *Marine Geochemistry*, 2nd ed., edited by H. D. Schulz and M. Zabel, pp. 391–427, Springer, Berlin.
Hedges, J. I., and R. G. Keil (1995), Sedimentary organic matter preservation: An assessment and speculative synthesis, *Mar. Chem.*, *49*, 81–115.
Helly, J. J., and L. A. Levin (2004), Global distribution of naturally occurring marine hypoxia on continental margins, *Deep Sea Res., Part I*, *51*, 1159–1168.
Homoky, W. B., S. Severmann, J. McManus, W. M. Berelson, T. E. Riedel, P. J. Statham, and R. A. Mills (2012), Dissolved oxygen and suspended particles regulate the benthic flux of iron from continental margins, *Mar. Chem.*, *134–135*, 59–70.
Homoky, W. B., S. G. John, T. M. Conway, and R. A. Mills (2013), Distinct iron isotopic signatures and supply from marine sediment dissolution, *Nat. Commun.*, *4*, 2143, doi:10.1038/ncomms3143.
Honeyman, B. D., and P. H. Santschi (1991), Coupling adsorption and particle aggregation: Laboratory studies of "colloidal pumping" using ^{59}Fe-labeled hematite, *Environ. Sci. Technol.*, *25*, 1739–1747.
Honeyman, B. D., L. S. Balistrieri, and J. W. Murray (1988), Oceanic trace metal scavenging: The importance of particle concentration, *Deep Sea Res.*, *35*, 227–246.
Inthorn, M., T. Wagner, G. Scheeder, and M. Zabel (2006), Lateral transport controls distribution, quality, and burial of organic matter along continental slopes in high-productivity areas, *Geology*, *34*, 205–208.
Jahnke, R. A., C. E. Reimers, and D. B. Craven (1990), Intensification of recycling of organic matter at the sea floor near ocean margins, *Nature*, *348*, 50–54.
Jeandel, C., B. Peucker-Ehrenbrink, M. T. Jones, C. R. Pearce, E. H. Oelkers, Y. Godderis, F. Lacan, O. Aumont, and T. Arsouze (2011), Ocean margins: The missing term in oceanic element budgets?, *Eos Trans. AGU*, *26*, 217–224, doi:10.1029/2011EO260001.
Jickells, T. D., et al. (2005), Global iron connections between desert dust, ocean biogeochemistry, and climate, *Science*, *308*, 67–71.
John, S. G., J. Mendez, J. Moffett, and J. Adkins (2012), The flux of iron and iron isotopes from San Pedro Basin sediments, *Geochim. Cosmochim. Acta*, *93*, 14–29.
Johnson, K. S., F. P. Chavez, and G. E. Friederich (1999), Continental-shelf sediment as a primary source of iron for coastal phytoplankton, *Nature*, *398*, 697–700.
Kriest, I., and A. Oschlies (2008), On the treatment of particulate organic matter sinking in large-scale models of marine biogeochemical cycles, *Biogeosciences*, *5*, 55–72.
Lam, P. J., J. K. B. Bishop, C. C. Henning, M. A. Marcus, G. A. Waychunas, and I. Y. Fung (2006), Wintertime phytoplankton bloom in the subarctic Pacific supported by continental margin iron, *Global Biogeochem. Cycles*, *20*, GB1006, doi:10.1029/2005GB002557.
Levin, L. A., and J. D. Gage (1998), Relationships between oxygen, organic matter and the diversity of bathyal macrofauna, *Deep Sea Res., Part II*, *45*, 129–163.
Lewandowski, J., C. Laskov, and M. Hupfer (2007), The relationship between *Chironomus plumosus* burrows and the spatial distribution of pore-water phosphate, iron and ammonium in lake sediments, *Freshwater Biol.*, *52*, 331–343.

Liu, K.-K., L. Atkinson, R. Quiñones, and L. Talaue-McManus (2010), *Carbon and Nutrient Fluxes in Continental Margins: A Global Synthesis*, 741 pp., Springer, Berlin.
Lohan, M. C., and K. W. Bruland (2008), Elevated Fe(II) and dissolved Fe in hypoxic shelf waters off Oregon and Washington: An enhanced source of iron to coastal upwelling regimes, *Environ. Sci. Technol.*, *42*, 6462–6468.
Luo, C., N. Mahowald, T. Bond, P. Y. Chuang, P. Artaxo, R. Siefert, Y. Chen, and J. Schauer (2008), Combustion iron distribution and deposition, *Global Biogeochem. Cycles*, *22*, GB1012, doi:10.1029/2007GB002964.
Mahowald, N. M., A. R. Baker, G. Bergametti, N. Brooks, R. A. Duce, T. D. Jickells, N. Kubilay, J. Prospero, and I. Tegen (2005), Atmospheric global dust cycle and iron inputs to the ocean, *Global Biogeochem. Cycles*, *19*, GB4025, doi:10.1029/2004GB002402.
Martin, J. H. (1990), Glacial-interglacial CO_2 change: The iron hypothesis, *Paleoceanography*, *5*, 1–13, doi:10.1029/PA005i001p00001.
Martin, J. H., and S. E. Fitzwater (1988), Iron deficiency limits phytoplankton growth in the north-east Pacific subarctic, *Nature*, *331*, 341–343.
McManus, J., W. M. Berelson, K. H. Coale, K. S. Johnson, and T. E. Kilgore (1997), Phosphorus regeneration in continental margin sediments, *Geochim. Cosmochim. Acta*, *61*, 2891–2907.
Meile, C., and P. Van Cappellen (2003), Global estimates of enhanced solute transport in marine sediments, *Limnol. Oceanogr.*, *48*, 777–786.
Meile, C., P. Berg, P. Van Cappellen, and K. Tuncay (2005), Solute-specific pore water irrigation: Implications for chemical cycling in early diagenesis, *J. Mar. Res.*, *64*, 601–621.
Menard, H. W., and S. M. Smith (1966), Hypsometry of ocean basin provinces, *J. Geophys. Res.*, *71*, 4305–4325, doi:10.1029/JZ071i018p04305.
Middelburg, J. J. (1989), A simple rate model for organic matter decomposition in marine sediments, *Geochim. Cosmochim. Acta*, *53*, 1577–1581.
Middelburg, J. J., and L. A. Levin (2009), Coastal hypoxia and sediment biogeochemistry, *Biogeosciences*, *6*, 1273–1293.
Middelburg, J. J., K. Soetaert, and P. M. J. Herman (1997), Empirical relationships for use in global diagenetic models, *Deep Sea Res., Part I*, *44*, 327–344.
Misumi, K., K. Lindsay, J. K. Moore, S. C. Doney, F. O. Bryan, D. Tsumune, and Y. Yoshida (2014), The iron budget in ocean surface waters in the 20th and 21st centuries: Projections by the Community Earth System Model version 1, *Biogeosciences*, *11*, 33–55.
Moore, J. K., and O. Braucher (2008), Sedimentary and mineral dust sources of dissolved iron to the world ocean, *Biogeosciences*, *5*, 631–656.
Moore, J. K., and S. C. Doney (2007), Iron availability limits the ocean nitrogen inventory stabilizing feedbacks between marine denitrification and nitrogen fixation, *Global Biogeochem. Cycles*, *21*, GB2001, doi:10.1029/2006GB002762.
Moore, J. K., S. C. Doney, and K. Lindsay (2004), Upper ocean ecosystem dynamics and iron cycling in a global three-dimensional model, *Global Biogeochem. Cycles*, *18*, GB4028, doi:10.1029/2004GB002220.
Nickelsen, L., D. Keller, and A. Oschlies (2015), Including a dynamic marine iron cycle in the University of Victoria Earth System Climate Model, *Geosci. Model Dev.*, *8*, 1357–1381, doi:10.5194/gmd-8-1357-2015.
Noffke, A., C. Hensen, S. Sommer, F. Scholz, L. Bohlen, T. Mosch, M. Graco, and K. Wallmann (2012), Benthic iron and phosphorus fluxes across the Peruvian oxygen minimum zone, *Limnol. Oceanogr.*, *57*, 851–867.
Pakhomova, S. V., P. O. J. Hall, M. Y. Kononets, A. G. Rozanov, A. Tengberg, and A. V. Vershinin (2007), Fluxes of iron and manganese across the sediment-water interface under various redox conditions, *Mar. Chem.*, *107*, 319–331.
Palastanga, V., C. P. Slomp, and C. Heinze (2013), Glacial-interglacial variability in ocean oxygen and phosphorus in a global biogeochemical model, *Biogeosciences*, *10*, 945–958.
Parekh, P., M. J. Follows, and E. Boyle (2004), Modeling the global ocean iron cycle, *Global Biogeochem. Cycles*, *18*, GB1002, doi:10.1029/2003GB002061.
Parekh, P., M. J. Follows, S. Dutkiewicz, and T. Ito (2006), Physical and biological regulation of the soft tissue carbon pump, *Paleoceanography*, *21*, PA3001, doi:10.1029/2005PA001258.
Poulton, S. W., and R. Raiswell (2002), The low-temperature geochemical cycle of iron: From continental fluxes to marine sediment deposition, *Am. J. Sci.*, *302*, 774–805.
Poulton, S. W., M. D. Krom, and R. Raiswell (2004), A revised scheme for the reactivity of iron (oxyhydr)oxide minerals towards dissolved sulfide, *Geochim. Cosmochim. Acta*, *68*, 3703–3715.
Radic, A., F. Lacan, and J. W. Murray (2011), Iron isotopes in the seawater of the equatorial Pacific Ocean: New constraints for the oceanic iron cycle, *Earth Planet. Sci. Lett.*, *306*, 1–10.
Raiswell, R., and D. E. Canfield (1998), Sources of iron for pyrite formation in marine sediments, *Am. J. Sci.*, *298*, 219–245.
Rickard, D., and G. W. Luther III (2007), Chemistry of iron sulfides, *Chem. Rev.*, *107*, 514–562.
Scholz, F., C. Hensen, A. Noffke, A. Rohde, V. Liebetrau, and K. Wallmann (2011), Early diagenesis of redox-sensitive trace metals in the Peru upwelling area—Response to ENSO-related oxygen fluctuations in the water column, *Geochim. Cosmochim. Acta*, *75*, 7257–7276.
Scholz, F., S. Severmann, J. McManus, and C. Hensen (2014a), Beyond the Black Sea paradigm: The sedimentary fingerprint of an open-marine iron shuttle, *Geochim. Cosmochim. Acta*, *127*, 368–380.
Scholz, F., J. McManus, A. C. Mix, C. Hensen, and R. Schneider (2014b), The impact of ocean deoxygenation on iron release from continental margin sediments, *Nat. Geosci.*, *7*, 433–437.
Severmann, S., J. McManus, W. M. Berelson, and D. E. Hammond (2010), The continental shelf benthic iron flux and its isotope composition, *Geochim. Cosmochim. Acta*, *74*, 3984–4004.
Sigman, D. M., and E. A. Boyle (2000), Glacial/interglacial variations in atmospheric carbon dioxide, *Nature*, *407*, 859–869.
Soetaert, K., J. J. Middelburg, P. M. J. Herman, and K. Buis (2000), On the coupling of benthic and pelagic biogeochemical models, *Earth Sci. Rev.*, *51*, 173–201.
Tagliabue, A., T. Mtshali, O. Aumont, A. R. Bowie, M. B. Klunder, A. N. Roychoudhury, and S. Swart (2012), A global compilation of dissolved iron measurements: Focus on distributions and processes in the Southern Ocean, *Biogeosciences*, *9*, 2333–2349, doi:10.5194/bg-9-2333-2012.
Tagliabue, A., O. Aumont, and L. Bopp (2014), The impact of different external sources of iron on the global carbon cycle, *Geophys. Res. Lett.*, *41*, 920–926, doi:10.1002/2013GL059059.
Teal, L. R., M. T. Bulling, E. R. Parker, and M. Solan (2008), Global patterns of bioturbation intensity and mixed depth of marine soft sediments, *Aquat. Biol.*, *2*, 207–218.
Thullner, M., A. W. Dale, and P. Regnier (2009), Global-scale quantification of mineralization pathways in marine sediments: A reaction-transport modeling approach, *Geochem. Geophys. Geosyst.*, *10*, Q10012, doi:10.1029/2009GC002484.
Van Cappellen, P., and Y. Wang (1996), Cycling of iron and manganese in surface sediments: A general theory for the coupled transport and reaction of carbon, oxygen, nitrogen, sulfur, iron, and manganese, *Am. J. Sci.*, *296*, 197–243.
Wang, Y., and P. Van Cappellen (1996), A multicomponent reactive transport model of early diagenesis: Application to redox cycling in coastal marine sediments, *Geochim. Cosmochim. Acta*, *60*, 2993–3014.

Weber, K. A., L. A. Achenbach, and J. D. Coates (2006), Microorganisms pumping iron: Anaerobic microbial iron oxidation and reduction, *Nat. Rev. Microbiol.*, *4*, 752–764.

Westrich, J. T., and R. A. Berner (1984), The role of sedimentary organic matter in bacterial sulfate reduction: The G-model tested, *Limnol. Oceanogr.*, *29*, 236–249.

Wu, J., and E. Boyle (2002), Implications for the processes controlling dissolved Fe distribution in the ocean, *Global Biogeochem. Cycles*, *16*(4), 1086, doi:10.1029/2001GB001453.